Parametric Study of Extended Brinkman's-Darcy Model for Triple Diffusive Convection System under the Effect of Rotational Modulation: Bifurcation Analysis

[1]Pervinder Singh, [1]Shruti Tomar, [2]Naresh M Chadha, [3]Vinod K. Gupta
Department of Mathematics, School of Physical Sciences,
DIT University, Dehradun−248009, INDIA

ABSTRACT
In this study, we consider the extended Brinkman's-Darcy model for a triple diffusive convection system which consists of some parameters such as Taylor number (Ta), Solutal Rayleigh numbers (R_{C_1}, R_{C_2}), and Prandtl number (Pr). To investigate the range of these parameters, a dynamical system of the Ginzburg-Landau equation is developed. The parametric analysis and comparative study of the model for the three Rayleigh numbers which leads to the clear fluid layer, sparsely packed porous layer, and densely packed porous layer is done with the help of bifurcation maps and the Lyapunov exponents. It is found that for a certain range of parameters, the system exhibits a chaotic behaviour.

Keywords: The extended Brinkman 's-Darcy model, Dynamical system, Bifurcation Maps, the Lyapunov Exponents, Chaotic behaviour.

Nomenclature

Latin Symbols

A	Amplitude of stream function
C_i	Concentration of i^{th} solute
g	Gravitational acceleration
g_0	Reference value of g
p	Atmospheric pressure
P_r	Prandtl number, $\nu/\kappa_{_T}$
$\vec{q}$	Fluid velocity (u, v, w)
R_T	Thermal Rayleigh number, $(g\Delta T d^3\alpha_{_T})/\nu\kappa_T$
R_{C_i}	i^{th} Solute Rayleigh number
Sh	Sherwood number
T	Temperature
V_a	Vadasz Number
Nu	Nusselt number
t	Time
τ	Rescaled time

Greek Symbols

$\alpha_{_T}$	Coefficient of Thermal expansion
β_{C_i}	Concentration expansion coefficient
γ	Heat capacity ratio
$\kappa_{_T}$	Thermal diffusivity $(\rho c_p)_m/(\rho c_p)_f$
$\kappa_{_{C_i}}$	Concentration diffusivity
τ_i	ratio of diffusivity,$\kappa_{_{C_i}}/\kappa_{_T}$
δ	Amplitude of modulation
ϵ	Perturbation parameter
ρ_0	Characteristic density
ρ	Density
k	Wave number
μ	Dynamic viscosity
ν	Kinematic viscosity
Ω	Frequency of modulation
ψ	Stream function

Other Symbols

b	Basic state
$'$	Perturbed state
$*$	Non-dimensional parameter

1. Introduction

The movement of heat or mass within a rotating fluid medium is referred to as convection in rotational flow. This phenomenon is frequently observed in both engineering applications, such as industrial mixing processes and geophysical fluid dynamics, and natural systems, such as the Earth's atmosphere and oceans[1]. The Coriolis effect applies to a rotating fluid, such as a spinning fluid in a container or the atmosphere of a revolving planet and stars [2]. The field of triple diffusive convection under rotation

studies the intricate fluid dynamics that result from a fluid undergoing rotation in addition to simultaneous gradients in temperature, salinity, and concentration (e.g., in a solution containing multiple solutes). Oceanography, astrophysics, and materials science are just a few of the natural and industrial processes that are impacted by this phenomenon. Lots of work under the rotational motion for triple diffusive convective system has been done by researchers in recent times. Some important research publications that explore this subject are [3–6].

Two primary components are the focus of the majority of triple diffusive convection research under rotational stress. The first is the linear effect or how the thermal Rayleigh number is used to interpret the onset of convection. The latter is the prediction of the non-linear effect that develops in the system after the start of convection, or how the rate of heat and mass transportation are explained. The expression of the thermal Rayleigh number for linear effect is obtained as a function of wave number and various parameters. Whereas the Ginzburg-Landau equation is derived to study non-linear effects; see[7–11]. To explain linear and non-linear effects, researchers analyze the system with fixed values of various parameters. Due to this the analysis of the system remains limited and incomplete to a great extent. A comparative analysis of triple diffusive convection systems under rotational modulation force for fixed values of different parameters, including solute Rayleigh number, Lewis number, Darcy number, and Taylor number, has been given by Singh *et al*[12]. In their study authors discussed the effect of amplitude of modulated rotational force as well as the effect of various parameters on the convective system.

As mentioned, fixed values of parameters make the study limited. Considering that the fixed value of parameters indicates a specific state of fluid. However, in real-world applications, any kind of fluid can be found, and the parameter value can fall anywhere in the range rather than being a fixed value. The range of parameters in which the system remains stable, i.e. the system does not exhibit chaos, is very important for real applications. Therefore, it is very important to determine the appropriate range of parameters for a more in-depth analysis of the convective system.

In order to examine how the range of parameters impacts the qualitative behaviour of the model, the most effective method is to conduct a bifurcation analysis. Bifurcation theory involves studying the qualitative changes in a system's state as a parameter is varied, and it can be utilized for both steady-state and dynamical systems. In this study, we utilize the dynamical system approach to investigate the range of parameters included in the model. Bifurcation analysis has many applications in various fields such as Plasma physics, Oceanography, Mathematical modelling, Transport problems etc.

The research conducted by Ghosh *etal*. [13] investigated a system comprising two fractional order differential equations that represent the dynamics of prey-predator interaction, taking into account intra-specific competition among predators. Through the utilization of bifurcation analysis, the study clarified the model's depiction of memory effect on population growth and shed light on the impact of memory-based growth on the global bifurcation threshold. In [14], Hosseini *et.al*. examined a generalized Schrödinger equation that describes the propagation of optical pulses in media. They obtained the dynamical system of the governing equation through the Galilean transformation and demonstrated the presence of chaotic behaviours within the system. Zhang *et.al*. [15] conducted a study on the Generalized Impulsive Kolmogorov model of pest and disease control using bifurcation analysis. Their research focused on examining the presence and overall stability of the semitrivial periodic solution of orders 1 and 2 through the establishment of a one-parameter family for the proposed system. For more details reader may go through [16–20] and reference therein.

In this article, we focus on the problem discussed in Singh *et al*[12] in which we aim to determine the range of different parameters that lead to either stability or instability within the system. To the best of the author's knowledge, no previous research of this kind has been conducted in this field. We also want to remind the reader that Singh's model has been used for all mathematical calculations in this study. Consequently, only the equations that must be proved in order to complete this research will be used in this paper. We will concentrate on the following issues in this study:

- To determine the range in which the system remains stable or unstable for the Taylor, solutal Rayleigh number, and Prandtl numbers under various media, such as clear, sparsely and densely packed porous layers.
- Using bifurcation analysis to analyse the chaotic nature of the convective system.

The article is organized as follows: In Section 2, the mathematical formulation of the model problem is presented. The linear stability analysis is conducted in Section 3, where the first-order solution of the model problem and three different values of the Rayleigh number are discussed in relation to the clear fluid, Darcy model, and Brinkman's model. The parametric analysis and comparative study of the model equation for all three values of the Rayleigh number are addressed in Section 4. The different stability nature of the system concerning these values is observed using bifurcation tools such as the study of equilibrium points, bifurcation maps, and the Lyapunov exponent plots. The conclusions are outlined in Section 5.

2. Mathematical Formulation

In the present problem we consider a horizontal layer of Newtonian fluid of depth d, heated and salted from below. Also, the layer of fluid is rotating anticlockwise with time-periodic modulated angular speed Ω about the vertical z-axis. Further, another solute salted from the free surface is also considered here. The temperature and concentration are greater at the lower boundary (z = 0) with respect to the upper boundary (z = d). we considered here a typical Cartesian system z-axis is vertically upward and the x and y-axis lie perpendicular to each other in the horizontal plane. Moreover, the Boussinesq approximation is used for the system which assumes that the variation in density with temperature and solute concentration is linear and the gravity is taken as the function of t for a very small time interval. The following equation provides a mathematical form of the current issue based on the fundamental principles of fluid dynamics Singh *et al*:

$$\nabla . q = 0 \tag{1}$$

$$\rho_0 \left[\frac{1}{\phi} \frac{\partial \vec{q}}{\partial t} + \frac{2}{\phi} (\vec{\Omega} \times \vec{q}) \right] + \frac{1}{\phi^2} (q.\nabla) q = -\nabla p + \rho \vec{g} - \lambda_2 \frac{\mu_f}{k} \vec{q} + \lambda_1 \mu_e \nabla^2 \vec{q} \tag{2}$$

$$\gamma \frac{\partial T}{\partial t} + \frac{1}{\phi} (\vec{q}.\nabla) T = k_{_T} \nabla^2 T \tag{3}$$

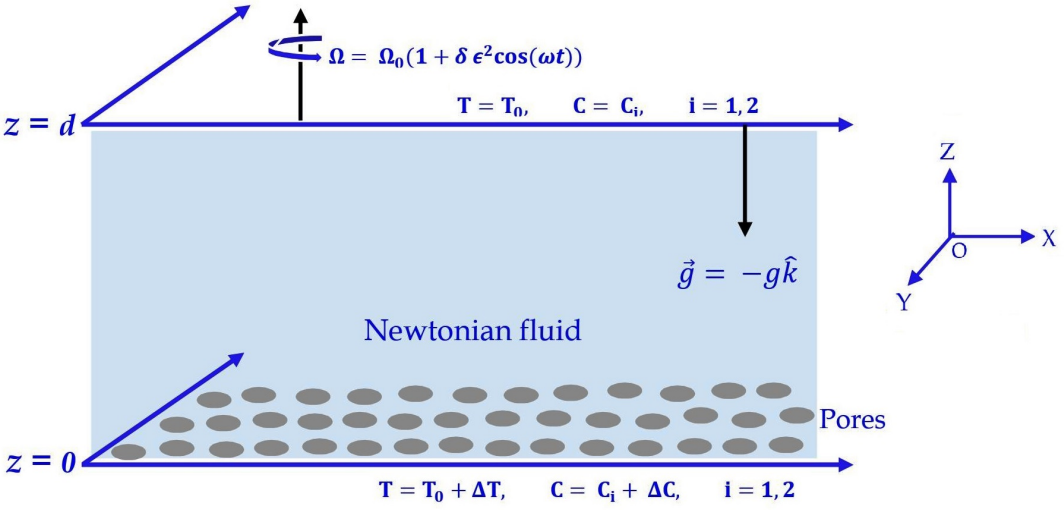

Figure 1. – Schematic Diagram.

$$\gamma_1 \frac{\partial C_1}{\partial t} + \frac{1}{\phi}(\vec{q}.\nabla)C_1 = k_1 \nabla^2 C_1 \tag{4}$$

$$\gamma_2 \frac{\partial C_2}{\partial t} + \frac{1}{\phi}(\vec{q}.\nabla)C_2 = k_2 \nabla^2 C_2 \tag{5}$$

All the quantities are defined in the nomenclature section. The Boussinesq equation with two concentrated solutes is given by

$$\rho = \rho_0 \left[1 - \alpha_T (T - T_0) + \beta_{C_1}(C_1 - C_{10}) + \beta_{C_2}(C_2 - C_{20})\right] \tag{6}$$

where, α_T, β_{C_1} and β_{C_2} are coefficients of thermal and concentration expansion respectively. The Modulation of Rotation is defined as

$$\Omega = \Omega_0[1 + \delta\epsilon^2 cos(\omega t)]\hat{k} \tag{7}$$

Thermal Boundary Conditions:

$$T(z,t) = \left\{ \begin{array}{ll} T_0 + \Delta T & at \quad z = 0 \\ T_0 & at \quad z = d \end{array} \right\} \tag{8}$$

Concentration Boundary Conditions:

$$C_1(z,t) = \left\{ \begin{array}{ll} C_{1_0} + \Delta C_1 & at \quad z = 0 \\ C_{1_0} & at \quad z = d \end{array} \right\} \tag{9}$$

$$C_2(z,t) = \left\{ \begin{array}{ll} C_{2_0} + \Delta C_2 & at \quad z = 0 \\ C_{2_0} & at \quad z = d \end{array} \right\} \tag{10}$$

After using a non-dimensional process, eliminating the pressure term, and utilising the basic state of the fluid, equations (2) through (5) have the following structure.

$$\Big(\frac{1}{Va}\frac{\partial}{\partial t}+\lambda_2\Big)\nabla^2\psi^*-\lambda_1 MD_a\nabla^4\psi^*-\frac{1}{Va}\frac{\partial(\psi^*,\nabla^2\psi^*)}{\partial(x^*,z^*)}+\sqrt{T_a}\frac{\partial v^*}{\partial z^*}=$$

$$-R_T\frac{\partial T^*}{\partial x^*}+R_{C_1}\frac{\partial T^*}{\partial x^*}+R_{C_2}\frac{\partial T^*}{\partial x^*}-\sqrt{T_a}(\epsilon^2\delta cos(\omega t))\frac{\partial v^*}{\partial z^*} \tag{11}$$

$$\frac{1}{Va}\frac{\partial v^*}{\partial t^*}-\frac{1}{Va}\frac{\partial(\psi^*,v^*)}{\partial(x^*,z^*)}+\sqrt{T_a}\frac{\partial\psi^*}{\partial z^*}-\lambda_2 v^*=\lambda_1 MD_a\nabla^2 v^*+\sqrt{T_a}(\epsilon^2\delta\cos\omega t^*)\frac{\partial\psi^*}{\partial z^*} \tag{12}$$

$$\gamma\frac{\partial T^*}{\partial t^*}-\frac{\partial(\psi^*,T^*)}{\partial(x^*,z^*)}-w^*=\nabla^2 T^* \tag{13}$$

$$\gamma_1\frac{\partial {C_1}^*}{\partial t^*}-\frac{\partial(\psi^*,{C_1}^*)}{\partial(x^*,z^*)}-w^*=\tau_{_1}\nabla^2{C_1}^* \tag{14}$$

$$\gamma_2\frac{\partial {C_2}^*}{\partial t^*}-\frac{\partial(\psi^*,{C_2}^*)}{\partial(x^*,z^*)}-w^*=\tau_{_2}\nabla^2{C_2}^* \tag{15}$$

Where, * denotes non-dimensional form of variables

3. Linear stability analysis

Now using the time variation for slow time scale that is $\tau=\epsilon^2 t^*$ then In matrix form equations (11) to (15) are written as

$$LX=B \tag{16}$$

where,

$$L=\begin{bmatrix}(-\lambda_2+\lambda_1 MD_a\nabla^2)\nabla^2 & -R_d\frac{\partial}{\partial x} & R_T\frac{\partial}{\partial x} & R_2\frac{\partial}{\partial x} & \sqrt{T_a}\frac{\partial}{\partial z}\\ -\sqrt{T_a}\frac{\partial}{\partial z} & 0 & 0 & 0 & (\lambda_2+\lambda_1 MD_a)\nabla^2\\ -\frac{\partial}{\partial x} & \nabla^2 & 0 & 0 & 0\\ -\frac{\partial}{\partial x} & 0 & \tau_1\nabla^2 & 0 & 0\\ -\frac{\partial}{\partial x} & 0 & 0 & \tau_2\nabla^2 & 0\end{bmatrix} \tag{17}$$

$$X = \begin{bmatrix} \psi \\ v \\ T \\ C_1 \\ C_2 \end{bmatrix} \; and \;\; B = \begin{bmatrix} \frac{-1}{V_a}\left[\epsilon^2 \frac{\partial}{\partial \tau}\nabla^2\psi + J(\psi, \nabla^2\psi)\right] - \sqrt{T_a}\epsilon^2\delta\cos(\omega t)\frac{\partial v}{\partial z} \\ \frac{\epsilon^2}{V_a}\frac{\partial v}{\partial \tau} - \frac{1}{V_a}J(\psi, v) - \sqrt{T_a}\epsilon^2\delta\cos(\omega t)\frac{\partial v}{\partial z} \\ \gamma\epsilon^2\frac{\partial T}{\partial \tau} + J(\psi, T) \\ \gamma_1\epsilon^2\frac{\partial C_1}{\partial \tau} + J(\psi, C_1) \\ \gamma_2\epsilon^2\frac{\partial C_2}{\partial \tau} + J(\psi, C_2) \end{bmatrix} \tag{18}$$

where $J(@, *)$ denotes the Jacobian with respect to x and z. For equation (33) the modulation is assumed to be very small to obtain the Ginzburg-Landau equation. Further, to perform weakly non-linear stability analysis, we have adopted the asymptotic expansions method. So, stream function ψ, temperature T, v, R_T, C_1 and C_2 are expanded in the form:

$$\xi = \sum_{n=1}^{\infty} \epsilon^n \xi_n, R_T = \sum_{n=0}^{\infty} \epsilon^{2n} R_{T_{2n}}, \tag{19}$$

where, $\xi = \psi, v, T, C_1, C_2$, It is also noted that the expansion of $R_{_T}$ contains only the even powers. Because changing the sign of ϵ only shifts the time origin, which does not affect the stability condition. Therefore the odd powers of ϵ are neglected here.

3.1. *First Order Solution*

To obtain the first-order solution, we compared the coefficients of ϵ on both sides of eqs.(33) and using the above expansion we get the following equations.

$$\begin{bmatrix} \nabla^4 - \lambda_2 & -R_T\frac{\partial}{\partial x} & R_{C_1}\frac{\partial}{\partial x} & R_{C_1}\frac{\partial}{\partial x} & \sqrt{T_a}\frac{\partial}{\partial z} \\ \sqrt{T_a}\frac{\partial}{\partial z} & 0 & 0 & 0 & (\lambda_2 - \lambda_1 MD_a)\nabla^2 \\ -\frac{\partial}{\partial x} & \nabla^2 & 0 & 0 & 0 \\ -\frac{\partial}{\partial x} & 0 & \tau_{_1}\nabla^2 & 0 & 0 \\ -\frac{\partial}{\partial x} & 0 & 0 & \tau_{_2}\nabla^2 & 0 \end{bmatrix} \begin{bmatrix} \psi_1 \\ v_1 \\ T_1 \\ C_{11} \\ C_{21} \end{bmatrix} = \begin{bmatrix} 0 \\ 0 \\ 0 \\ 0 \\ 0 \end{bmatrix} \tag{20}$$

The convection cells exhibit periodic behaviour in both the x and z directions, as well as being a function of time. Therefore, we propose a time-dependent periodic solution in the x and z directions as outlined below.

$$\psi_1 = \mathcal{A}(\tau)\sin(kx)\sin(\pi z), \tag{21}$$

$$T_1 = \mathcal{B}(\tau)\cos(kx)\sin(\pi z), \tag{22}$$

$$C_1 = \mathcal{C}(\tau)\cos(kx)\sin(\pi z), \tag{23}$$

$$C_2 = \mathcal{D}(\tau)\cos(kx)\sin(\pi z), \tag{24}$$

$$v_1 = \mathcal{E}(\tau)\sin(kx)\cos(\pi z), \tag{25}$$

and obtained the solution according to the boundary conditions:

$$\psi_1 = \mathcal{A}(\tau)\sin(kx)\sin(\pi z), \tag{26}$$

$$T_1 = -\frac{k}{p^2}\mathcal{A}(\tau)\cos(kx)\sin(\pi z), \tag{27}$$

$$C_{11} = -\frac{k}{p^2\tau_1}\mathcal{A}(\tau)\cos(kx)\sin(\pi z), \tag{28}$$

$$C_{21} = -\frac{k}{p^2\tau_2}\mathcal{A}(\tau)\cos(kx)\sin(\pi z), \tag{29}$$

$$v_1 = \frac{-\pi\sqrt{T_a}D_a}{(\lambda_2 + \lambda_1 M D_a p^2)}\mathcal{A}(\tau)\sin(kx)\cos(\pi z), \tag{30}$$

where,

$$p^2 = k^2 + \pi^2 \tag{31}$$

At this stage, we obtained critical thermal Darcy Rayleigh numbers for stationary and oscillatory modes of the onset of convection.

$$R_{T_0} = \frac{\lambda_1 D_a M p^6}{k^2} + \frac{\lambda_2 p^4}{k^2} + \frac{R_{C_1}}{\tau_1} - \frac{R_{C_2}}{\tau_2} + \frac{T_a D_a \pi^2 p^2}{k^2(\lambda_2 + \lambda_1 D_a M p^2)} \tag{32}$$

Case I: In the context of a Clear Fluid Layer, the parameters are defined as $\lambda_1 = 1$, $\lambda_2 = 0$, and $M = 1$. The critical Rayleigh number is also specified as follows:

$$R^f_{T_0} = \frac{D_a p^6}{k^2} + \frac{R_{C_1}}{\tau_1} + \frac{R_{C_2}}{\tau_2} + \frac{T_a \pi^2}{k^2} \tag{33}$$

The term $R^f_{T_0}$ refers to the critical Rayleigh number applicable solely to the fluid layer. This value is considered to be at its minimum, denoted as R_{T_0}, when k equals k_c, with k_c fulfilling the subsequent equation.

$$(k_c^2)^3 + \frac{3\pi^2}{2}(k_c^2)^2 - \frac{\pi^2}{2}(T_a + \pi^4) \tag{34}$$

Case II: The Darcy Model pertains to a densely packed porous layer of fluid. In this scenario, the parameters are defined as follows: $\lambda_1 = 0$, $\lambda_2 = 1$, and $M = 1$. Additionally, the Rayleigh number is specified as follows:

$$R^D_{T_0} = \frac{p^4}{k^2} + \frac{R_{C_1}}{\tau_1} - \frac{R_{C_2}}{\tau_2} + \frac{T_a D_a \pi^2 p^2}{k^2} \tag{35}$$

Case III: Brinkman's Model pertains to a sparsely packed porous layer of fluid. In this scenario, both λ_1 and λ_2 are equal to 1, and the Rayleigh number is specified as follows

$$R^B_{T_0} = \frac{MD_a p^6}{k^2} + \frac{p^4}{k^2} + \frac{R_{C_1}}{\tau_1} - \frac{R_{C_2}}{\tau_2} + \frac{T_a \pi^2 p^2}{k^2(D_a^{-1} + Mp^2)} \tag{36}$$

where $R^B_{T_0}$ denotes the value of the thermal Darcy Rayleigh number for the Brinkman-Darcy porous medium.

3.1.1. Critical Value of Rayleigh number

Since we consider the Brinkman's - Darcy medium for convection, Therefore to obtain the critical value of Rayleigh number for the onset of convection, we have $\lambda_1 = 1$ and $\lambda_2 = 1$. Also for the critical value of R_{T_0}, we use the following condition on equation (32).

$$R'_{T_0}(x) = 0 \tag{37}$$

$$\Rightarrow \frac{d}{dx}\left[\lambda_1 \frac{M(x+a)^3}{x} + \lambda_2 \frac{M(x+a)^2}{Dax} - \frac{\pi^2 T_a (x+a)}{D + M(x+a)}\right] = 0 \tag{38}$$

where $x = k_c^2$, taking $X = \pi^2 + k_c^2$ and using the above condition we obtained the following equation.

$$a_5 X^5 + a_4 X^4 + a_3 X^3 + a_2 X^2 + a_1 X + a_0 = 0 \tag{39}$$

where, $a_5 = 2M^3 Da$, $a_4 = 5M^2 - \pi^2 M^3 Da$, $a_3 = 4MDa^{-1} - 4\pi^2 M^2$

$a_2 = \pi^2 MTa(2 + \pi^2) + {D_a}^{-2} - 5\pi^2 MDa^{-1}$ $a_1 = -(2\pi^2 {D_a}^{-2} + \pi^2 MTa(1 + \pi^2))$

$a_0 = -\pi^4 TaDa^{-1}$

4. Bifurcation Analysis of Ginzburg Landau Equation

In this section, we will perform a bifurcation analysis of time-dependent autonomous Ginzburg Landau equation obtained by Singh *et al* in their model. This aims to identify the range of parameters where the system demonstrates chaotic behaviour using the Ginzburg Landau equation's coefficients. Consider the following Ginzburg Landau equation obtained by Singh *et al*[12]

$$\alpha_0 A'(\tau) - \alpha_1(\tau) A(\tau) - \alpha_2 A^3(\tau) = 0. \tag{40}$$

The corresponding dynamical system is

$$A^{'}(\tau) = \frac{1}{\alpha_0}\left(\alpha_1(\tau)A(\tau) + \alpha_2 A^3(\tau)\right). \tag{41}$$

where,

$$\begin{aligned}
\alpha_0 &= \frac{p^2}{Pr} - \frac{\pi^2 Ta}{Pr(\lambda_2 Da^{-1} + \lambda_1 Mp^2)} - \frac{k^2}{p^4}(Ra_{t0} + Le_1^2 Rc_1 - Le_2^2 Rc_2);\\
\alpha_1 &= -\frac{k^2 Rt_2}{p^2} - \frac{2\pi^2 Ta(\delta\cos(\omega\tau)}{\lambda_2 Da^{-1} + \lambda_1 Mp^2};\\
\alpha_2 &= \frac{k^4}{8p^4}(Ra_{t0} - Rc_1 Le_1^3 + Rc_2 Le_2^3) - \frac{\pi)^4 k^2 Ta}{((Da^{-1}+p^2)^2)(\lambda_2 Da^{-1}) + 4\lambda_1 Mk^2)}.
\end{aligned} \tag{42}$$

Corresponding equilibrium points are $E_{1,2} = \left[0, \sqrt{\frac{\alpha_1}{\alpha_0}}\right]$. With respect to these equilibrium points, the nature of the dynamical system Equation 41 is given below in Table 1.

Eq. Pts	Eigenvalues	Conditions	Nature	
0	$\lambda = \frac{\alpha_1}{\alpha_0}$	$\alpha_1 > 0, \alpha_0 < 0$	$\lambda < 0$	Stable
		$\alpha_1 > 0,\ \alpha_0 > 0$	$\lambda > 0$	Unstable
$\sqrt{\frac{\alpha_1}{\alpha_2}}$	$\lambda = \frac{-\alpha_1}{\alpha_0}$	$\alpha_1 > 0, \alpha_0 < 0$	$\lambda > 0$	Unstable
		$\alpha_1 > 0,\ \alpha_0 > 0$	$\lambda < 0$	Stable

Table 1. – Nature of the Dynamical system Equation 41 with respect to different equilibrium points $E_1 = 0$ and $E_2 = \sqrt{\frac{\alpha_1}{\alpha_2}}$.

Applying the bifurcation theory, it is clear from Table 1 that the system will become unstable with respect to the first equilibrium point E_1 if $\alpha_1 > 0$ and $\alpha_0 > 0$, are both positive coefficients. Whereas, it will become stable for the same values of the coefficients for the second equilibrium point E_2. But if we choose $\alpha_1 > 0$ and $\alpha_0 < 0$ for the first equilibrium point E_1, the system becomes stable and for the second equilibrium point E_2, it shows instability with respect to the opposite combinations of the coefficients values. Here can be other combinations to get the stable and unstable behaviour of the dynamical system Equation 41.

Determining the characteristics of the dynamic system described by the differential Equation 1 in relation to its coefficients is challenging due to the fact that another set of parameters also influences these coefficients. The study of a dynamical system concerning each parameter will become more complex, hence we are considering some specific parameters such as Rc_1, Rc_2, Ta, and Pr for further investigation.

Figure 2 shows two specific regions with respect to the nature of the coefficient α_0. With the help of the above stability analysis in Table 1, for a set value of $[Pr, Rc_1] \in [0.001, 30] \times [50, 600]$, the region-1 shows the stability space for the dynamical system Equation 41 at $\alpha_0 < 0$ and the region-2 indicates that the dynamical system will be unstable in this region at $\alpha_0 > 0$, shown in Figure 2 (a). Whereas, the Figure 2 (b) shows that the behaviour of the dynamical system will be stable in region-1 and unstable in region-2 with respect to another set values of the parameters $[Rc_1, Rc_2] \in [50, 600] \times [100, 600]$.

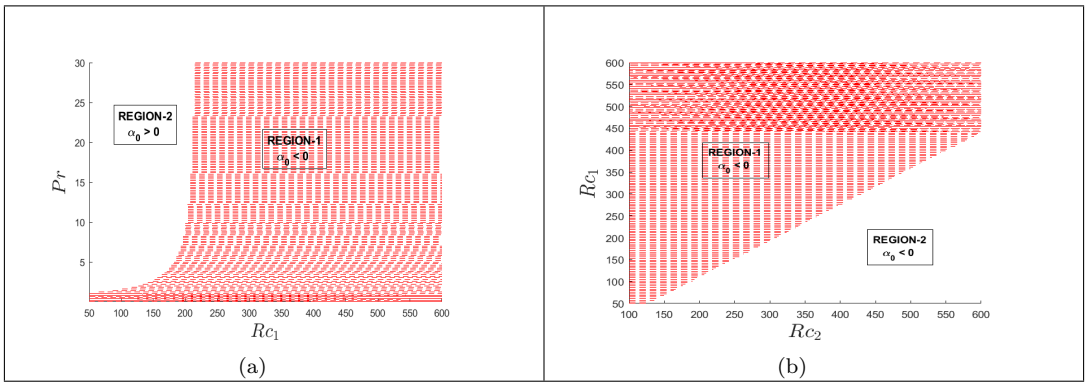

Figure 2. – Region plots for the nature of the coefficient α_0 with respect to the set values of parameters (a) $[Pr, Rc_1] \in [0.001, 30] \times [50, 600]$ and (b) $[Rc_1, Rc_2] \in [50, 600] \times [100, 600]$.

By utilizing these figures, we have identified a range of parameters that show different behaviours of the dynamical system Equation 41, including stability and instability. However, the duration for which this dynamical system remains stable across a range of parameters is uncertain. A seemingly stable system may actually be in a state of chaos. In order to investigate this scenario, we have analyzed the bifurcation maps and Lyapunov exponent plots in the next section.

4.1. *Bifurcation maps and Lyapunov Exponent*

In this section, we compare the stability region with respect to the three different cases of Rayleigh number with the help of bifurcation maps and the Lyapunov exponent plots.

4.1.1. Comparison for the three cases of Rayleigh number

Case I: Clear Fluid Layer, In this case $\lambda_1 = 1$ and $\lambda_2 = 0$, $M = 1$ and the value of critical Rayleigh number is

$$R^f_{T_0} = \frac{D_a p^6}{k^2} + \frac{R_{C_1}}{\tau_1} + \frac{R_{C_2}}{\tau_2} + \frac{T_a \pi^2}{k^2} \tag{43}$$

Case II: Darcy Model i.e for a densely packed porous layer of fluid, In this case, $\lambda_1 = 0$ and $\lambda_2 = 1$, $M = 1$ and the value Rayleigh number is

$$R^D_{T_0} = \frac{p^4}{k^2} + \frac{R_{C_1}}{\tau_1} - \frac{R_{C_2}}{\tau_2} + \frac{T_a D_a \pi^2 p^2}{k^2} \tag{44}$$

Case III: Brinkman's Model i.e for a sparsely packed porous layer of fluid, In this case, $\lambda_1 = 1$ and $\lambda_2 = 1$, and the value Rayleigh number is

$$R^B_{T_0} = \frac{M D_a p^6}{k^2} + \frac{p^4}{k^2} + \frac{R_{C_1}}{\tau_1} - \frac{R_{C_2}}{\tau_2} + \frac{T_a \pi^2 p^2}{k^2 (D_a^{-1} + M p^2)} \tag{45}$$

where $R^B_{T_0}$ denotes the value of the thermal Darcy Rayleigh number for the Brinkman-

Darcy porous medium.

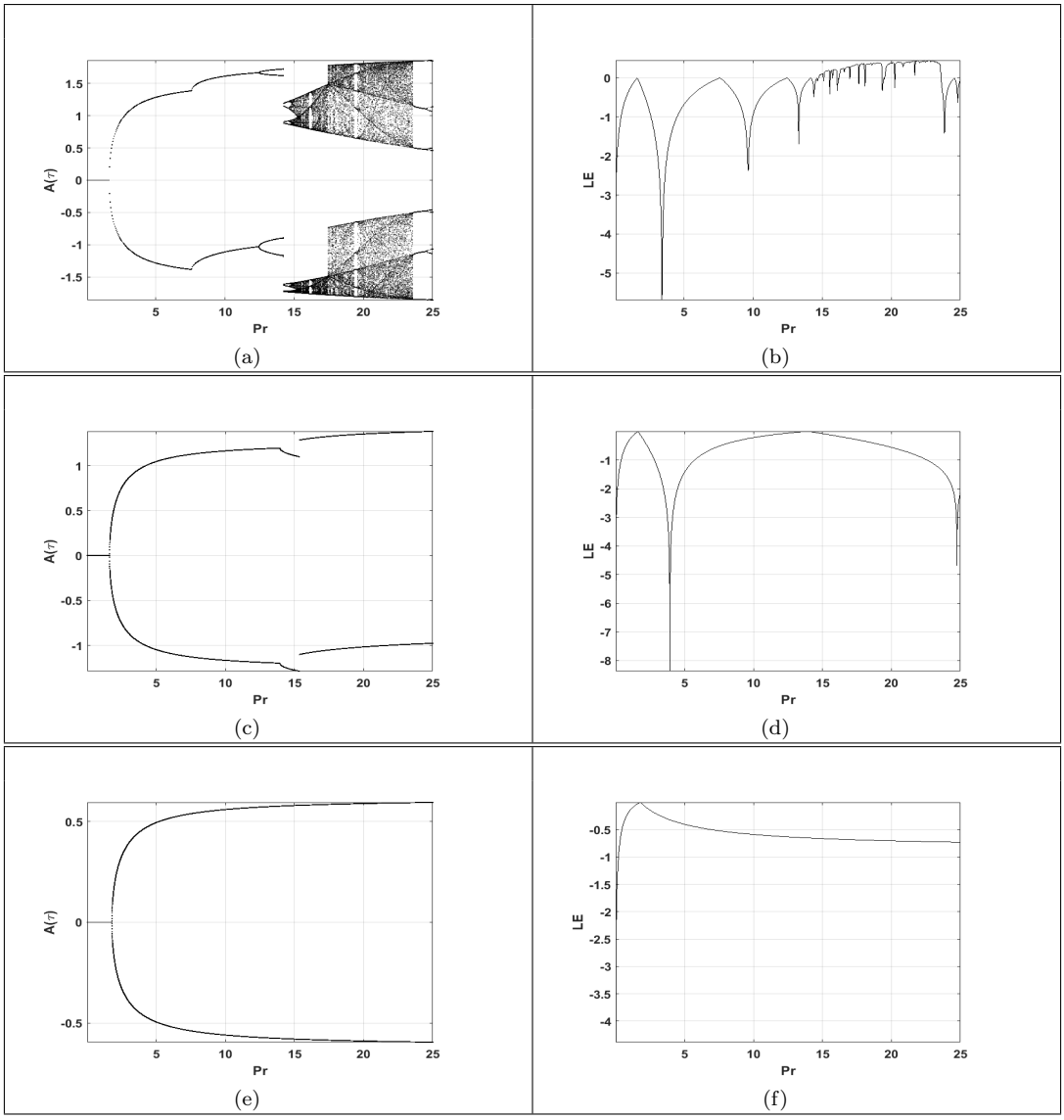

Figure 3. – Bifurcation map and Lypunov plot for the range of the Pr number $Pr \in [0, 25]$, $Da = 0.05; Rc_2 = 300; \delta = 0.5; Le_1 = 1.8; Le_2 = 1.6; p = (k^2 + \pi^2)^{0.5}; Rc_1 = 310; Ta = 80; \omega = 2; \tau = 2; M = 1; \lambda_1 = 1; \lambda_2 = 0;$.

As the present study is for Newtonian fluid, hence in the present paper the range Prandtl number ($0.001 \leq Pr \leq 25$) has been considered to be the one which is consistent with Newtonian fluid. Figure 3 (a), (c), and (e) shows the bifurcation maps for the range of the parameters $Pr \in [0.001, 25]$. The figures (a) and (b) represent the bifurcation map and the Lyapunov exponent plot for the clear fluid layer. The figure (a) depicts that for a certain value of the parameter Pr, the system exhibits stable behaviour. Whereas, after crossing a certain region, the behaviour of the dynamical system of the model problem Equation 41 becomes unpredictable and shows chaotic behaviour. The visible white slits are called the periodic windows in this chaotic region in which the system undergoes stability for certain values of the parameter Pr. Thus, for the clear fluid layer, the system shows chaotic behavior for Pr ¿ 15. Consequently,

it may be concluded that the system is headed towards chaos as long as the system's momentum diffusivity dominates its heat diffusivity.

Further from figures (c) and (e) it depict the bifurcations maps for Darcy and Brinkman-Darcy model corresponding to the sparsely and densely packed porous layer respectively. It is found that the clear fluid layer in the convective system exhibits the highest chaotic pattern, less for the sparsely fluid layer and the lowest for the densely fluid layer within the fixed range of Pr. Which means that excess of porosity in the system provides stability to the system.

To confirm this, we employ Lyapunov exponents. In principle, the Lyapunov exponents are the average exponential rates of divergence or convergence of orbits or trajectories originating from neighbouring initial points [21, 22]. The positive value of the Lyapunov exponent plot shows the existence of chaos in the system and for the negative value, the system becomes stable [23–26]. Figure 3 (b) shows the positive values of the Lyapunov exponent for a certain range of the parameter Pr which indicates the chaotic behaviour of the dynamical system in this region. Whereas figures (d), and (f) show the negative value for a range of parameter for which the system shows the stability. When the value of the Lyapunov exponent becomes zero, the single periodic line bifurcates itself into a double of previous ones. In the figure (c), the value of the Lyapunov exponent becomes zero twice. Therefore, the bifurcation map shows the double periodic and four periodic behaviour for the range of parameter Pr. Whereas, in the figure (e), the Lyapunov exponent becomes zero once. Therefore, the bifurcation maps show double periodicity which indicates more stability in the system as compared to the previous ones.

Bifurcation maps for different fluid layers for the parameter R_{C_1}, which corresponds to the concentration of the first solute C_1, are shown in Figure 4. From Figure 4(a), it is noted that the system only shows chaotic behaviour for the clear fluid layer within $200 \leq R_{C_1} \leq 250$. However for $R_{C_1} > 250$ the system attains stability. Next, Figure 4(c) depict the chaotic pattern of Darcy fluid layer with respect to R_{C_1}. In this case it is observed that the system only shows chaotic behaviour for the clear fluid layer within $200 \leq R_{C_1} \leq 200$. However for $R_{C_1} > 200$ the system attains stability. Further from Figure 4(e), it evident that the chaotic behaviour of the system for Brinkmann-Darcy porous layer become less as compare to previous cases and approaches its end when $R_{C_1} > 220$. As we have assumed a positive downward concentration gradient of solute C_1 along the z-axis for the purposes of this particular scenario. Consequently, increasing R_{C_1} results in the system becoming more stable for all three types of fluid layers. Aside from that, the clear fluid layer achieves stability last, while the dense fluid layer achieves stability first.

Next, Figure 5 demonstrates system stability with the second solute C_2. From which it is observed that with the increase of R_{C_2}, the system exhibits chaos around $R_{C_2} = 300$ for the clear fluid layer. For a densely packed porous layer i.e. Darcy medium this chaos body achieves $R_{C_2} \geq 325$. Whereas for a densely packed porous layer i.e. Brinkmann–Darcy model this chaos for $R_{C_2} \geq 350$. Because solute C_2 has a negative gradient downward along the z-axis, it is important to observe that the impact of R_{C_2} is opposite to that of R_{C_1}.

Figure 5 display the opposite behaviour in all three cases. Within the range $Rc_1 \in [200, 600]$, Figure 4 (a) displays the instability for a specific range of this parameter. We have observed that every time the value of the Lyapunov exponent becomes zero, the periodic window becomes double the previous window. The Figure 4 $(b), (d)$, and (f) reflect zero so often that it creates chaos for a small range of the parameter which is visible in Figure 4 $(a), (c)$, and (e). We have seen that for increasing values of the

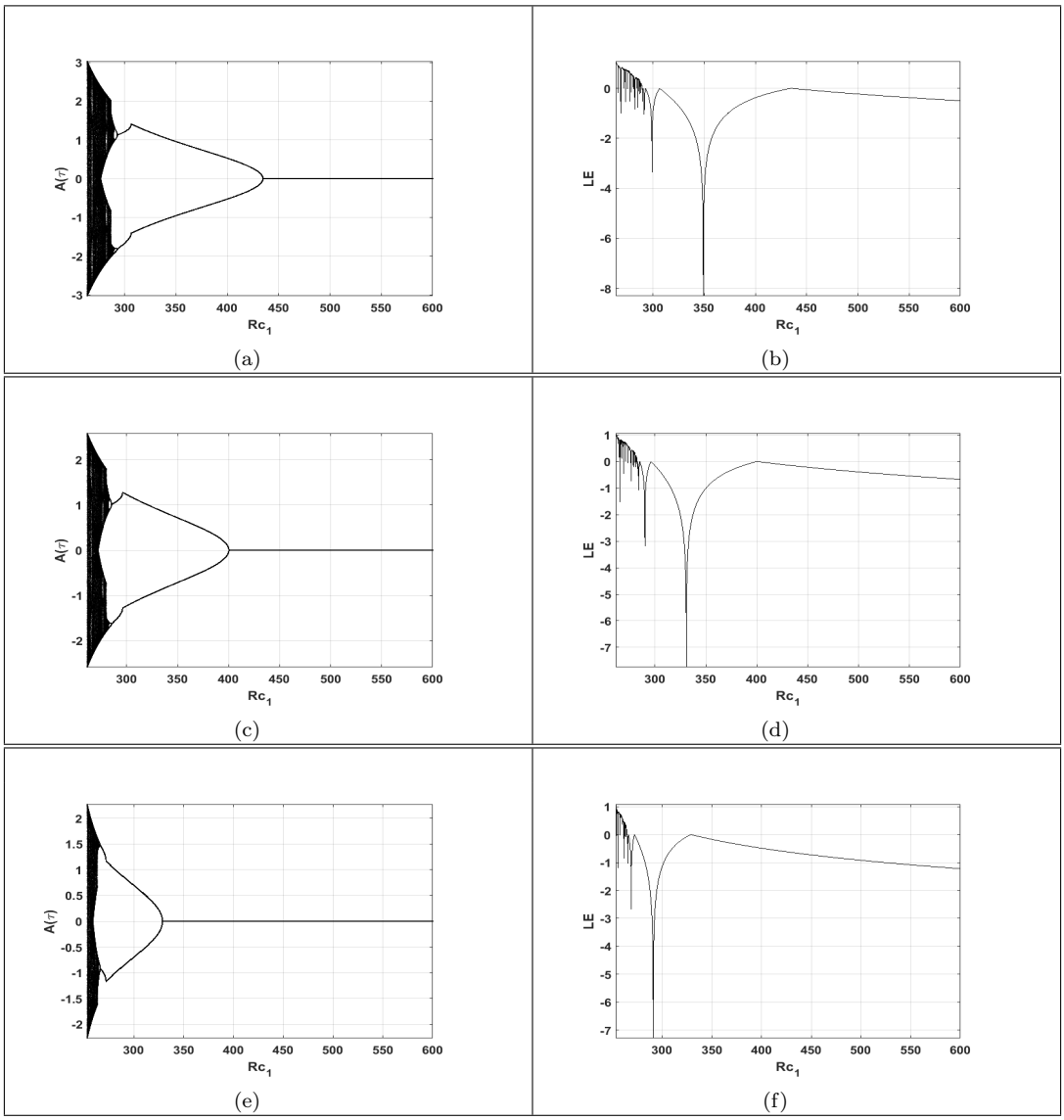

Figure 4. – Bifurcation map and Lypunov plot for the range of $Rc_1 \in [200, 600]$, $Da = 0.05; Rc_2 = 300; \delta = 0.5; Le_1 = 1.8; Le_2 = 1.6; p = (k^2 + \pi^2)^{0.5}; Pr = 6.9; Ta = 80; \omega = 2; \tau = 2; M = 1; \lambda_1 = 1; \lambda_2 = 0;$..

parameter the system comes out of the chaotic region. It shows a transition to a double periodic and then a single periodic region. In this region, the system becomes stable, which is supported by the negative values of the Lyapunov exponent shown in Figure 4 $(b), (d)$, and (f). Therefore the increasing values of this parameter $R_{C_2} \in [100, 400]$, the system first shows stable behaviour and finally converges to the chaotic region. This can be justified by the first negative values of the Lyapunov exponent and further conversion to positive values, shown in Figure 5 $(b), (d)$, and (f). The same sequence of all three cases for the thermal Rayleigh number has been taken here as discussed above.

Figure 6 $(a), (c), (e)$ shows the bifurcation maps of the system for all three models with Taylor number (Ta). For first two cases namely clear fluid layer and Sparsely packed porous layer it is observe that system shows chaos when Ta increases. However

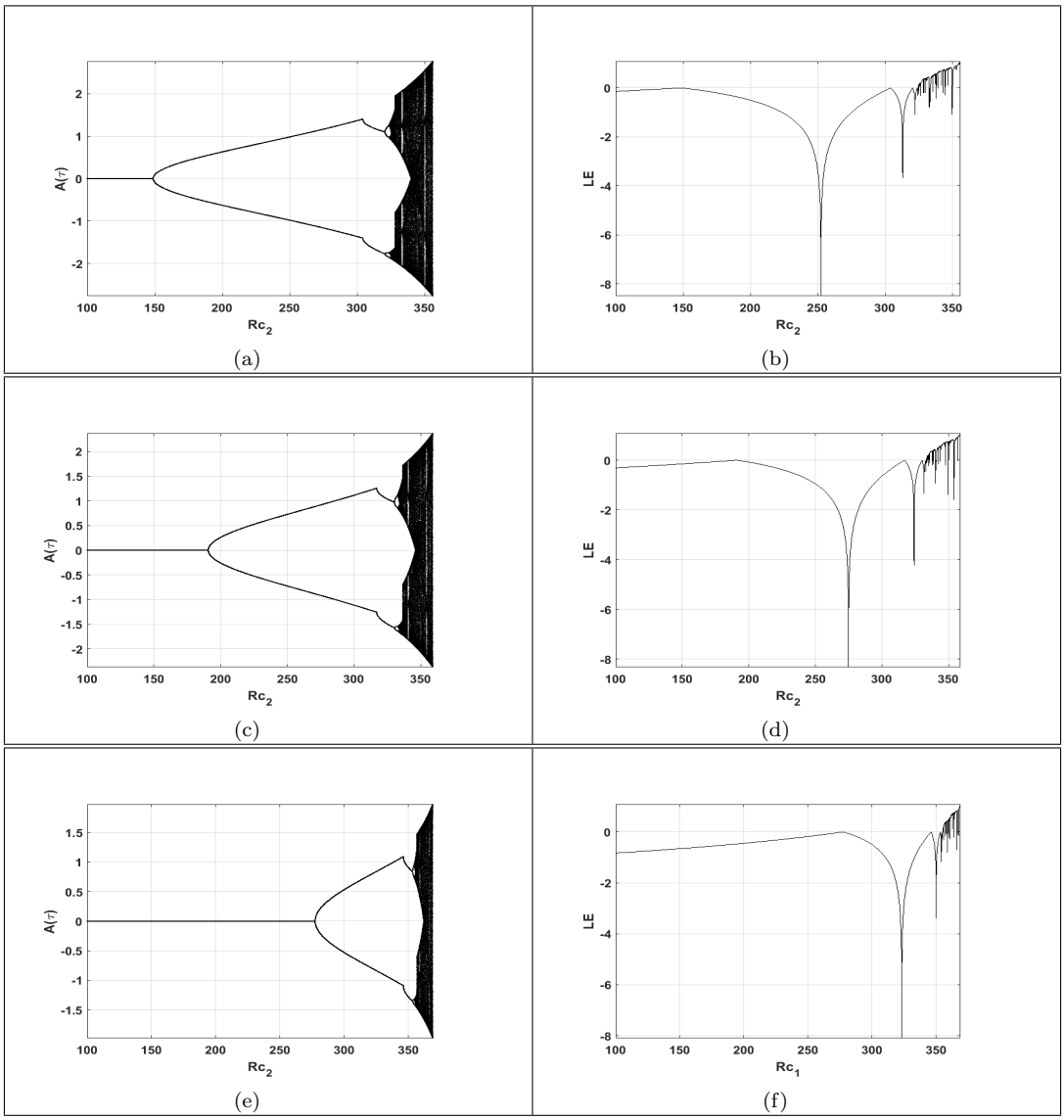

Figure 5. – Bifurcation map and Lypunov plot for the range of $R_{C_2} \in [100, 400]$, $Da = 0.05; \delta = 0.5; Le_1 = 1.8; Le_2 = 1.6; p = (k^2 + \pi^2)^{0.5}; R_{C_1} = 310; Ta = 80; Pr = 6.9; \omega = 2; \tau = 2; M = 1; \lambda_1 = 1; \lambda_2 = 0;$.

for clear fluid layer the system exhibiting chaotic behavior for $Ta > 140$. However, for Darcy medium with Ta, this chaos begins after $Ta > 170$. In contrast to the two aforementioned cases the Brinkmann-Darcy model does not exhibit chaotic behavior in the system until Ta = 200. This indicates that the system with the clear fluid layer loses stability first, followed by the system with the sparsely packed porous layer, while the system with the densely packed porous layer remains stable as the rotation rate increases. Consequently, it is conclude that the system's porosity prevents the effects of excessive rotation and gives it stability.

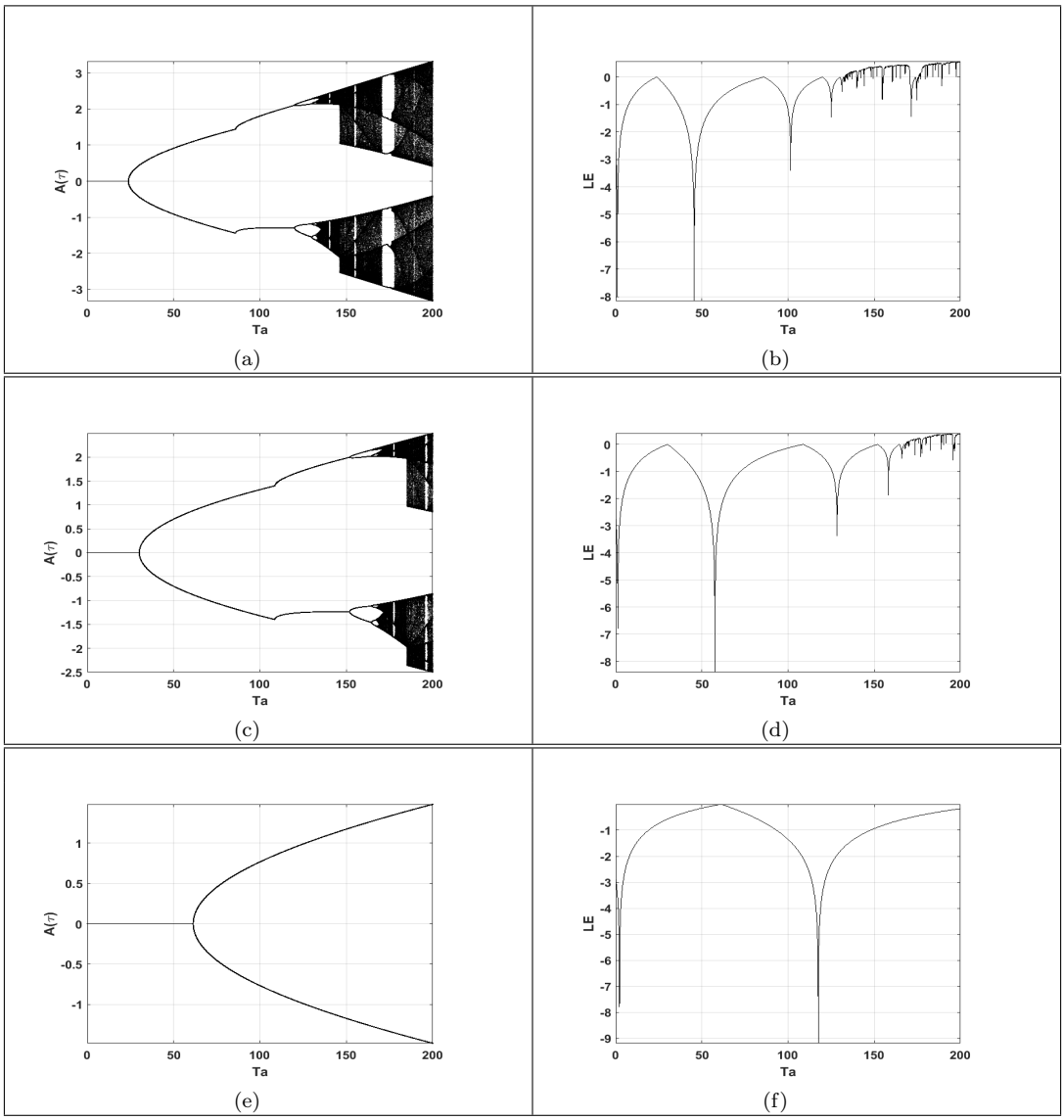

Figure 6. – Bifurcation map and Lypunov plot for the range of $Ta \in [0, 200]$, $Da = 0.05; R_{C_2=300}; \delta = 0.5; Le_1 = 1.8; Le_2 = 1.6; p = (k^2 + \pi^2)^{0.5}; Rc_1 = 310; Pr = 6.9; \omega = 2; \tau = 2; M = 1; \lambda_1 = 1; \lambda_2 = 0;..$

5. Conclusions

In this work, the combined effects of two diffusive components (C1 and C2) salted in opposite directions and a modulated rotational speed were studied to determine the chaotic nature of Brinkman's-Darcy porous medium. The range of parameters (Pr, RC1, RC2, and Ta) in which the three types of fluid layers—the clear fluid layer, the densely packed porous layer, and the densely packed porous layer—show chaotic behaviour are identified using the bifurcation maps with Lyapunov exponent. Using MATLAB software, bifurcation maps of the Ginzburg Landau equation with various parameters have been plotted. Following a graph comparison analysis, we arrived at the following conclusion.

- The clear fluid layer becomes chaotic for Pr ¿ 15. In contrast, chaos is not observed in densely packed porous layers until Pr = 25. In other words, greater porosity helps lessen the impact of Pr.
- The system's chaotic behaviour decreases as the concentration of solute (C_1) in the bottom layer rises. Thus, the convective system is stabilised by the solute concentrated at the lower layer.
- The system's chaotic behaviour increases as the concentration of solute (C_2) in the upper layer rises. Thus, the convective system is destabilised by the solute concentrated at the upper layer.
- Compared to the sparsely and densely packed porous layers, the clear fluid layer system approaches chaotic behaviour more quickly as rotation speed increases.

References

[1] BM Boubnov and Georgi S Golitsyn. *Convection in rotating fluids*, volume 29. Springer Science & Business Media, 2012.

[2] RJ Tayler. Convection in rotating stars. *Monthly Notices of the Royal Astronomical Society*, 165(1):39–52, 1973.

[3] Suresh Chand. Effect of rotation on triple-diffusive convection in a magnetized ferrofluid with internal angular momentum saturating a porous medium. *Applied Mathematical Sciences*, 6(65):3245–3258, 2012.

[4] Suresh Chand. Effect of rotation on triple-diffusive convection in walters'(model b´) fluid in porous medium. *Research Journal of Science and Technology*, 5(1):184–188, 2013.

[5] Sameena Tarannum and S Pranesh. Heat and mass transfer of triple diffusive convection in a rotating couple stress liquid using ginzburg-landau model. *International Journal of Mechanical and Mechatronics Engineering*, 11(3):583–588, 2017.

[6] M Rudziva, P Sibanda, OAI Noreldin, and S Goqo. On trigonometric cosine, square, sawtooth, and triangular wave-type rotational modulations on triple-diffusive convection in salted water. *Heat Transfer*, 50(7):6886–6914, 2021.

[7] PG Siddheshwar, BS Bhadauria, and Alok Srivastava. An analytical study of nonlinear double-diffusive convection in a porous medium under temperature/gravity modulation. *Transport in porous media*, 91:585–604, 2012.

[8] Vinod K Gupta. Study of mass transport in rotating couple stress liquid under concentration modulation. *Chinese journal of physics*, 56(3):911–921, 2018.

[9] Pervinder Singh and Vinod K Gupta. Simultaneous action of modulated temperature and third diffusing component on natural convection. In *International workshop of Mathematical Modelling, Applied Analysis and Computation*, pages 209–231. Springer, 2022.

[10] Pervinder Singh, Vinod K Gupta, Isaac Lare Animasaun, Taseer Muhammad, and Qasem M Al-Mdallal. Dynamics of newtonian liquids with distinct concentrations due to time-varying gravitational acceleration and triple diffusive convection: Weakly non-linear stability of heat and mass transfer. *Mathematics*, 11(13):2907, 2023.

[11] Pervinder Singh, Jogendra Kumar, and BS Bhadauria. Weakly non-linear stability analysis of g-jitter induced rayleigh–bénard convection under inclined surfaces. *Chinese Journal of Physics*, 91:525–537, 2024.

[12] Pervinder Singh, Vinod K Gupta, and Naresh M Chadha. Study of heat and

mass transports due to modulated rotational flow in a triply diffusive newtonian liquid saturated porous medium/fluid layer: A comparative study. *International Journal of Heat and Fluid Flow*, 108:109449, 2024.

[13] Uttam Ghosh, Swadesh Pal, and Malay Banerjee. Memory effect on bazykin's prey-predator model: Stability and bifurcation analysis. *Chaos, Solitons Fractals*, 143:110531, 2021.

[14] Kamyar Hosseini, Evren Hinçal, and Mousa Ilie. Bifurcation analysis, chaotic behaviors, sensitivity analysis, and soliton solutions of a generalized schrödinger equation. *Nonlinear Dynamics*, 111(18):17455–17462, 2023.

[15] Qianqian Zhang, Biao Tang, Tianyu Cheng, and Sanyi Tang. Bifurcation analysis of a generalized impulsive kolmogorov model with applications to pest and disease control. *SIAM Journal on Applied Mathematics*, 80(4):1796–1819, 2020.

[16] Jinying Guo, Huailong Shi, Ren Luo, and Jing Zeng. Bifurcation analysis of a railway wheelset with nonlinear wheel–rail contact. *Nonlinear Dynamics*, 104(2):989–1005, 2021.

[17] Pankaj Kumar and S Narayanan. Chaos and bifurcation analysis of stochastically excited discontinuous nonlinear oscillators. *Nonlinear Dynamics*, 102:927–950, 2020.

[18] Asit Saha, Khalid K Ali, Hadi Rezazadeh, and Yogen Ghatani. Analytical optical pulses and bifurcation analysis for the traveling optical pulses of the hyperbolic nonlinear schrödinger equation. *Optical and Quantum Electronics*, 53:1–19, 2021.

[19] Shruti Tomar and Naresh M Chadha. Study of fixed points and chaos in wave propagation for the generalized damped forced korteweg-de vries equation using bifurcation analysis. *Chaos Theory and Applications*, 5(4):286–292, 2023.

[20] Shruti Tomar, Naresh M Chadha, and Ankita Khanna. A mathematical model to study regulatory properties and dynamical behaviour of glycolytic pathway using bifurcation analysis. In *Computational Methods for Biological Models*, pages 81–116. Springer, 2023.

[21] Shruti Tomar, Naresh M Chadha, and Santanu Raut. Bifurcation analysis of generalized damped forced kdv equation and its analytical solitary wave solutions. In *AIP Conference Proceedings*, volume 2852. AIP Publishing, 2023.

[22] Ndolane Sene. Qualitative analysis of class of fractional-order chaotic system via bifurcation and lyapunov exponents notions. *Journal of Mathematics*, 2021:1–18, 2021.

[23] Steven H Strogatz. *Nonlinear dynamics and chaos with student solutions manual: With applications to physics, biology, chemistry, and engineering*. CRC press, 2018.

[24] Jonathan B Dingwell. Lyapunov exponents. *Wiley encyclopedia of biomedical engineering*, 2006.

[25] Luís Barreira. *Lyapunov exponents*. Springer, 2017.

[26] Naresh M Chadha, Shruti Tomar, and Santanu Raut. Parametric analysis of dust ion acoustic waves in superthermal plasmas through non-autonomous kdv framework. *Communications in Nonlinear Science and Numerical Simulation*, 123:107269, 2023.